

Spatio-temporal dynamics behind the shock front from compacted metal nanopowders

Ch. Leela,¹ P. Venkateshwarlu,¹ Raja V. Singh,² Pankaj Verma,²
and P. Prem Kiran^{1,*}

¹Advanced Centre of Research in High Energy Materials (ACRHEM), University of Hyderabad, Hyderabad-500046, India

²High Energy Material Research Laboratory, Sutarwadi, Pune, Maharashtra-411021, India
premkiranuoh@gmail.com

Abstract: Laser ablated shock waves from compacted metal nanoenergetic powders of Aluminum (Al), Nickel coated Aluminum (Ni-Al) was characterized using shadowgraphy technique and compared with that from Boron Potassium Nitrate (BKN), Ammonium Perchlorate (AP) and Potassium Bromide (KBr) powders. Ablation is created by focused second harmonic (532 nm, 7 ns) of Nd:YAG laser. Time resolved shadowgraphs of propagating shock front and contact front revealed dynamics and the precise time of energy release of materials under extreme ablative pressures. Among the different compacted materials studied, Al nanopowders have maximum shock velocity and pressure behind the shock front compared to others.

©2014 Optical Society of America

OCIS codes: (100.0118) Imaging ultrafast phenomena; (160.0160) Materials; (110.2970) Image detection systems.

References and links

1. A. Ulas, G. A. Risha, and K. K. Kuo, "An investigation of the performance of a Boron/Potassium nitrate based pyrotechnic igniter," *Propellants Explosives Pyrotech.* **31**(4), 311–317 (2006).
2. Y. S. Kwon, A. A. Gromov, and J. I. Strokova, "Passivation of the surface of Aluminum nanopowders by protective coatings of the different chemical origin," *Appl. Surf. Sci.* **253**(12), 5558–5564 (2007).
3. M. A. Zamkov, R. W. Conner, and D. D. Dlott, "Ultrafast chemistry of nanoenergetic materials studied by time-resolved infrared spectroscopy: Aluminum nanoparticles in teflon," *J. Phys. Chem. C* **111**(28), 10278–10284 (2007).
4. D. E. Eakins and N. N. Thadhani, "The shock-densification behavior of three distinct Ni+Al powder mixtures," *Appl. Phys. Lett.* **92**(11), 111903 (2008).
5. S. Roy, N. Jiang, H. U. Stauffer, J. B. Schmidt, W. D. Kulatilaka, T. R. Meyer, C. E. Bunker, and J. R. Gord, "Spatially and temporally resolved temperature and shock-speed measurements behind a laser-induced blast wave of energetic nanoparticles," *J. Appl. Phys.* **113**(18), 184310 (2013).
6. N. K. Bourne, "Akrology: materials: physics in extremes," *AIP Conf. Proc.* **1426**, 1331–1334 (2012).
7. N. K. Bourne, J. C. F. Millett, and G. T. Gray III, "On the shock compression of polycrystalline metals," *J. Mater. Sci.* **44**(13), 3319–3343 (2009).
8. A. N. Ali, S. F. Son, B. W. Asay, and R. K. Sander, "Importance of the gas phase role to the prediction of energetic material behavior: an experimental study," *J. Appl. Phys.* **97**(6), 063505 (2005).
9. R. E. Russo, X. Mao, H. Liu, J. Gonzalez, and S. S. Mao, "Laser ablation in analytical chemistry—a review," *Talanta* **57**(3), 425–451 (2002).
10. D. Yarmolich, V. Vekselman, and Y. E. Krasik, "A concept of ferroelectric microparticle propulsion thruster," *Appl. Phys. Lett.* **92**(8), 081504 (2008).
11. J. E. Sinko and C. R. Phipps, "Modeling CO₂ laser ablation impulse of polymers in vapor and plasma regimes," *Appl. Phys. Lett.* **95**(13), 131105 (2009).
12. C. Phipps, M. Birkan, W. Bohn, H. A. Eckel, H. Horisawa, T. Lippert, M. Michaelis, Y. Rezunkov, A. Sasoh, W. Schall, S. Scharring, and J. Sinko, "Review: laser-ablation propulsion," *J. Propul. Power* **26**(4), 609–637 (2010).
13. S. L. Vummidi, Y. Aly, M. Schoenitz, and E. L. Dreizin, "Characterization of fine Nickel-coated Aluminum powder as potential fuel additive," *J. Propul. Power* **26**(3), 454–460 (2010).
14. S. Siano, G. Pacini, R. Pini, and R. Salimbeni, "Reliability of refractive fringe diagnostics to control plasma-mediated laser ablation," *Opt. Commun.* **154**(5–6), 319–324 (1998).
15. Ch. Leela, S. Bagchi, V. R. Kumar, S. P. Tewari, and P. P. Kiran, "Dynamics of laser induced micro-shock waves and hot core plasma in quiescent air," *Laser Particle Beams* **31**(02), 263–272 (2013).
16. L. I. Sedov, *Similarity and Dimensional Methods in Mechanics* (CRC, 1993).

17. S. H. Jeong, R. Greif, and R. E. Russo, "Propagation of the shock wave generated from Excimer laser heating of Aluminum targets in comparison with ideal blast wave theory," *Appl. Surf. Sci.* **127–129**, 1029–1034 (1998).
18. Ya. B. Zel'dovich and Yu. P. Raizer, *Physics of Shockwaves and High-Temperature Hydrodynamic Phenomena* (Dover, 2002).
19. P. Verma and R. V. Singh, HEMRL (Personal communication, 2012).
20. N. Zhang, X. N. Zhu, J. J. Yang, X. L. Wang, and M. W. Wang, "Time-resolved shadowgraphs of material ejection in intense femtosecond laser ablation of Aluminum," *Phys. Rev. Lett.* **99**(16), 167602 (2007).
21. H. L. Brode, "Numerical solutions of spherical blast waves," *J. Appl. Phys.* **26**(6), 766–775 (1955).
22. R. A. Freeman, "Variable-energy blast waves," *J. Phys. D Appl. Phys.* **1**(12), 1697–1710 (1968).
23. X. Chen, B. M. Bian, Z. H. Shen, J. Lu, and X. W. Ni, "Equations of laser-induced plasma shock wave motion in air," *Microw. Opt. Technol. Lett.* **38**(1), 75–79 (2003).
24. B. Wang, K. Komurasaki, T. Yamaguchi, K. Shimamura, and Y. Arakawa, "Energy conversion on a glass-laser-induced blast wave in air," *J. Appl. Phys.* **108**(12), 124911 (2010).
25. C. Porneala and D. A. Willis, "Time-resolved dynamics of nanosecond laser-induced phase explosion," *J. Phys. D Appl. Phys.* **42**(15), 155503 (2009).
26. D. Batani, H. Stabile, A. Ravasio, G. Lucchini, F. Strati, T. Desai, J. Ullschmied, E. Krousky, J. Skala, L. Juha, B. Kralikova, M. Pfeifer, Ch. Kadlec, T. Mocek, A. Präg, H. Nishimura, and Y. Ochi, "Ablation pressure scaling at short laser wavelength," *Phys. Rev. E Stat. Nonlinear Soft Matter Phys.* **68**(6), 067403 (2003).
27. S. Bagchi, P. P. Kiran, K. Yang, A. M. Rao, M. K. Bhuyan, M. Krishnamurthy, and G. R. Kumar, "Bright, low debris, ultrashort hard X-ray table top source using carbon nanotubes," *Phys. Plasmas* **18**(1), 014502 (2011).
28. S. Bagchi, P. P. Kiran, M. K. Bhuyan, S. Bose, P. Ayyub, M. Krishnamurthy, and G. R. Kumar, "Hot ion generation from nanostructured surfaces under intense femtosecond irradiation," *Appl. Phys. Lett.* **90**(14), 141502 (2007).

1. Introduction

Novel energetic materials have variety of applications in propellants, igniters, initiators in airbag gas generators, pyrotechnics etc. to name a few. For eg., Aluminum (Al) is used in rocket propellant formulations and also in combustion mechanism as it act as effective catalyst. Also Boron Potassium Nitrate (BKN) based pyrotechnic igniter is used as an initiator in airbag gas generator or propulsion. Due to the special properties of compacted powders, they are used in propellants, pyrotechnics, optical, biomedical and environmental engineering [1]. However, the major challenge is to reduce the hazardous emissions while the energetic materials undergo reactions converting the internal energy in to the kinetic energy for applications. Though variety of mechanisms was proposed to channelize the energy released, precise control of energy release from the energetic materials has been a challenging task. Nano energetic materials have started replacing the best known molecular explosives owing to the control of energy release by modifying the shape and size of the nanostructures [2–5]. Energetic Materials create temperatures and pressures of the order of 3000-10000 K and > 100 MPa respectively generally created under controlled laboratory conditions using Diamond Anvil Cell, shock tubes and gas guns [6,7] and rely heavily on the modeling and simulation to get overall reaction mechanism of the energy release. The development of high power table top laser systems associated with fast imaging techniques has given unique opportunity to study the kinetics of the material under extreme conditions, like phase transitions during energy release process of energetic materials with/without allowing propagation of chemical reaction, fragmentation, temperature during the reactions [3,5,8,9]. In addition, this approach allows us to control the energy extraction during the reactions. When the laser intensity is larger than the breakdown threshold of a specific material, a small portion of the material melts, evaporate and form a material plume. This plume expands and drives the background gas (in our case air) to a supersonic velocity forming a shock wave (SW). Understanding the evolution of SW has many applications out of which Laser ablation propulsion (LAP) is a new electric propulsion concept that gives a precise control over the environmentally hazardous emissions compared to chemical propulsion schemes and is being used in micro thruster applications [10–13]. Variety of materials such as metals (Al, Cu etc), polymers (PVC, triazene, polyvinyl alcohol, nitrocellulose, PVN, CH, CN, Nylon etc), polymeric CHO propellants, liquid layers on metal sheets excited with laser light of varying wavelength from UV to long IR regions of spectrum with varied pulse durations and modes were used for LAP [10–13]. In this paper, we present the evolution of laser ablative shockwaves (SWs) from compacted nanopowders of Al and Nickel coated Al to understand

the challenging aspects of laser-nanopowder interactions to explore their application potential for LAP [10,11]. To ensure the suitability of the compacted nanopowders for specific application, the results were compared with micron sized powders of Boron Potassium Nitrate (BKN), Ammonium Perchlorate (AP) and Potassium Bromide (KBr) compacted and studied under the same experimental conditions.

2. Experimental details

The evolution of laser ablated SWs from the compacted samples into surrounding air is studied using defocused shadowgraphy (SHW) imaging technique at different time delays after the shock inducing laser pulse. Defocused shadowgraphy gives not only the information about the expansion of plasma, propagation of shock front and ionization of vaporized material but also gives the information about the evolution of the dynamics of ejected mass from the ablated material getting converted into plasma that launches a shockwave in to the ambient medium [14,15]. The experimental schematic used in our study is depicted in Fig. 1(a). Second harmonic of Nd:YAG laser (INNOLAS Spitlight-1200) (532 nm, 7 ns, 10 Hz) is focused using a plano-convex lens of 80 mm focal length in $f/\#10$ geometry. The beam diameter at the focal plane is measured to be $140 \pm 10 \mu\text{m}$. The input laser energy is kept at 75 mJ per pulse leading to an intensity of $7 \times 10^{10} \text{ W/cm}^2$ on the surface of the sample. He-Ne laser (632.8 nm, CW, 25 mW, Thorlabs) was used as probe beam to capture the evolution of shock front (SF) and contact front (CF) in to the ambient atmosphere. The probe beam expanded to 15 mm captures the laser ablated SF and CF. As the probe beam passes through the plume, it gets refracted by a region with high density gradients causing dark and bright areas in the shadowgraphs.

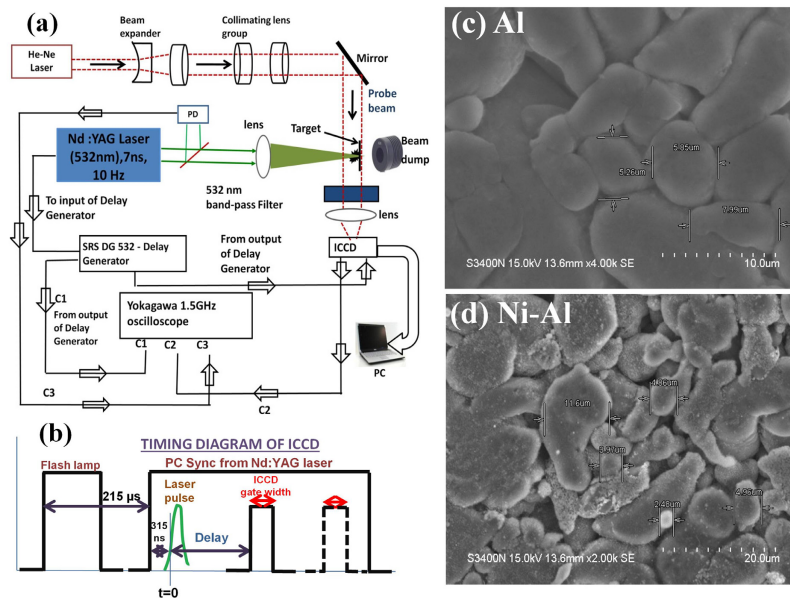


Fig. 1. (a) Experimental schematic of shadowgraphy, (b) synchronization of ICCD camera with the laser pulse, SEM images of compacted (c) Al and (d) Ni-Al nanopowders.

The variations created by laser ablated materials in ambient air were captured by probe beam using an ICCD camera (ANDOR DH-734 with a minimum gate width or temporal resolution of 1.5 ns and spatial resolution of $13 \mu\text{m}$ over 1024×1024 pixel array) was synchronized with the laser by triggering delay generator (SRS DG535) with Pockel's cell (PC) sync pulse from Nd: YAG laser. This allowed us to overcome the inherent insertion delay of the ICCD camera. The delay between laser pulse and ICCD gate width was adjusted by using delay generator. The beginning of the laser pulse is taken as $t = 0$. The output from

delay generator was used to trigger ICCD camera to ensure capturing evolution of plasma created by every laser pulse and starts acquiring images, allowing shadowgraphs to be taken at any desired time delay. PC pulse (C1), gate width of the ICCD (C2), laser pulse (C3) and the delay of the ICCD gate width from $t = 0$, were monitored using an oscilloscope (YOKOGAWA DL9240L, 1.5 GHz, 10 GS/s) (Fig. 1(b)). A band-pass filter transparent only to probe beam is placed in front of the ICCD camera to eliminate background illumination due to ns laser pulses. The images were captured at various time delays with an initial time delay of 400 ns. Time-resolved shadowgraphs are used to understand the SW evolution revealing position of SF [16–18] and expansion of hot gas (CF) respectively. The Al nanoparticles of 70–110 nm dimension were procured from Advanced Powder Technologies LLC, ALEX™. Nickel coating was done by an in house developed method [19] ensuring that a coating of 12 ± 3 nm was made on the nanoparticles. For the specific application of LAP and to compare with the regular energetic materials, the nanopowders were compacted under a load of 6 Tons to form pellets with dimensions of 1 inch in diameter and 1 mm thickness. Upon compaction the nanoparticles were observed to agglomerate giving a particle size in the range of 2–20 μm as shown in in Figs. 1(c) and 1(d) for Al and Ni-Al nanopowders, respectively, with uniform distribution of the particles along the material layer. The ablative shock waves from the compacted nano energetic powders were compared with that of BKN, AP and spectroscopic grade KBr powders compacted under the same conditions. The pellets were mounted on an electronically controlled XY translation stages (M-443, LTA-HA controlled by ESP-300, M/s. Newport) to ensure that fresh surface of the sample interacts with the laser pulse.

3. Results and discussion

The evolution of laser ablative shockwaves from the compacted powder pellets is compared. Figures 2(a)–2(f) show shadowgraphs for Al pellets at input laser energy of 75 mJ and time delays of 0.8, 2, 3.6, 5.6, 7.6 and 11.2 μs from $t = 0$ respectively.

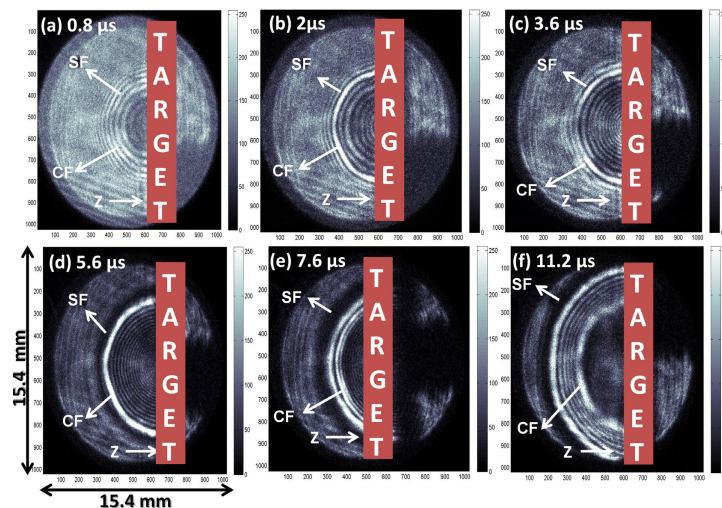


Fig. 2. Shadowgraphs showing shock front (SF) and contact front (CF) of Aluminum (Al) at a time delay of (a) 0.8 μs (b) 2 μs (c) 3.6 μs (d) 5.6 μs (e) 7.6 μs and (f) 11.2 μs at 75 mJ input laser energy.

Each image has a spatial extent of 15.4 mm \times 15.4 mm with a spatial resolution of ~ 15 μm (calibrated by imaging the output from a single mode optical fiber and comparing with a high resolution beam profiler with SP620U, Ophir Spiricon). The laser propagation direction (z) is from left to right. At each time delay, ten images were captured and averaged to obtain shock propagation distance (R_{SW}). Each of the images captured during the SW process was imported

in to MATLAB® software and analyzed to extract the position of SF. After the calibration of the captured image was performed, the radius of the shock front (R_{SW}) was measured for different pellets (Fig. 3(f)). The laser ablated material is observed to evolve with varying density gradients (as shown by a series of bright and dark fringes in Figs. 2(a)–2(f)) till 3–6 μ s. From the images, SW (outer discontinuous dark layer due to the changes in the refractive index caused mainly by the high density gradients) and the Contact Front (CF) (a white thick layer) which separates the ambient gas from material vapor generated by ablation can be seen clearly. Around 4 μ s, a dark band representing compressed air detaches from the evolving ablated plasma and is launched in to quiescent air as SF. Two sets of fringes were located internally and externally with respect to the SW were observed. The interference between undisturbed probe rays passing out of the SW and those deflected by the shock rear produces the internal fine fringes, while the external ones are due to the interference between the slightly perturbed rays and those deflected by the shock leading front [14]. The emergence of internal fringes were observed until a time delay of 3–6 μ s after which the fringes disappear once the SF (dark layer) gets detached from contact front of Fig. 2(d) leading to the oscillations of CF. Similar diffraction pattern of light and dark stripes at the earlier time scales of the ablation has been reported earlier [5,20]. These were attributed to the conversion of material in the solid phase into the gaseous phase [5] and due to intermittent material ejection at high temperatures [20].

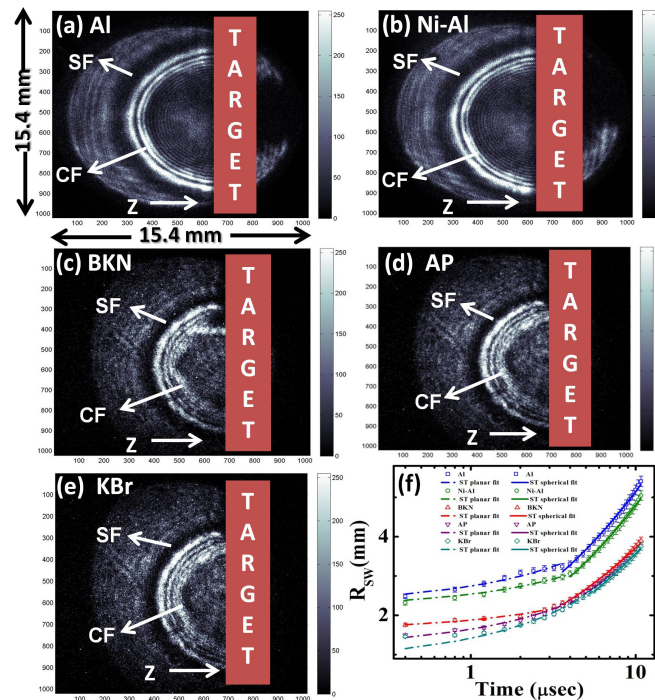


Fig. 3. Shadowgraphs showing Shock Front (SF) and Contact Front (CF) at 7.6 μ s delay from the laser pulse for (a) Aluminum (Al) (b) Nickel coated Aluminum (Ni-Al) (c) Boron Potassium Nitrate (BKN) (d) Ammonium perchlorate (AP) (e) potassium Bromide (KBr) and (f) Radius of curvature of shock front (SF) (R_{SW}) at 75 mJ input laser energy. Lines are fit to the data using the CPC-PSET model for the hemispherical shockwave evolution from the targets.

At around 7 μ s, a secondary shock layer is observed to get detached from the contact front and propagate into the ambient atmosphere. The evolution of time dependent shock front is observed to be different for different targets. Figures 3(a)–3(e) show shadowgraphs at 7.6 μ s delay from $t = 0$ for Aluminum (Al), Nickel coated Aluminum (Ni-Al), Boron Potassium Nitrate (BKN), Ammonium perchlorate (AP) and potassium Bromide (KBr) targets

respectively. Time dependent evolution of shockfront has been explained using variety of models beginning from Sedov-Taylor's (S-T) classical Point Strong Explosion Theory (PSET) explaining the propagation in planar, cylindrical and spherical geometry [16–18], to the ones considering gas motion in Lagrangian form for spherical [21] and cylindrical [22] variable energy blast waves, laser induced plasma shock wave motion in air [23,24], laser induced phase explosions of solid targets [20,25] and gas phase effects in energetic materials [5]. PSET assumes that energy deposited at a point source propagates through the medium as a shockwave where the energy is released at a distance which is extremely large. From the temporal evolution of R_{SW} , the energy released in the explosion that drives the SW (E_s) and the nature of the SF expansion is estimated using the relation $R_{SW} = \phi_0 [E_s t^2 / \rho_0]^{1/(n+2)}$, where t is the time elapsed since the origin of the disturbance that generated the SW, ρ_0 is the density of the ambient medium (1.184 Kg/m^3) and ϕ_0 is a constant dependent upon the specific heat ratio, γ (1.4), of the ambient medium [8–10] (SW nature: if $n = 1$ planar, $n = 2$ cylindrical and $n = 3$ spherical). In our experimental configuration, as we have used pellets, hemispherical SW's are observed for all the targets. Hence, the energy driving the hemispherical SW $E_h = 0.5 E_s$. The evolution of the R_{SW} from the compacted powders is observed to follow two different slopes indicating two specific stages of evolution before and after the detachment of SF from CF (Fig. 3(f)). At the earlier times up to 2 – 3 μs , the variation of R_{SW} is minimal (within 200 – 800 μm) for all the samples studied and observed to follow a planar nature. After the detachment from CF, SF is observed to accelerate faster into the ambient medium following spherical Sedov-Taylor solution. The faster acceleration of SF indicates the time scales around which phase explosions of the material from the nascent phase to the vapor phase occur [25]. The lines in Fig. 3(f) show the fit to the experimental data obtained using the CPC-PSET model for the hemispherical shockwave evolution from the targets. At earlier time scales S-T planar expansion (dash-dot lines) and at latter time scales S-T spherical expansion (solid dash) is observed [17,25]. At all the time scales, the acceleration of SF from compacted metal nanopowders (Al, Ni-Al) is observed to be faster compared to the other powders. The energy driving the hemispherical shock waves, E_h (in mJ) estimated by the fits is observed to be higher for Al followed by Ni-Al, BKN, AP and KBr.

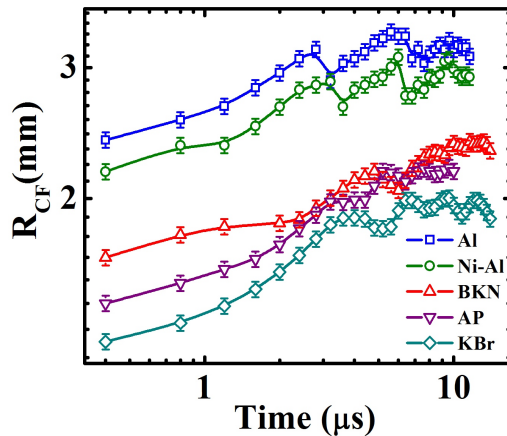


Fig. 4. Evolution of radius of contact front (R_{CF}) from compacted nanopowders at 75 mJ of incident laser energy. Lines are guide to the eye.

To understand the observed anomalous shock front behavior, the temporal evolution of contact front (R_{CF}) that gives information about the expansion of the ejected mass [17] and believed to be the source of energy released was also studied for time delays up to 12 μs from $t = 0$ (Fig. 4). The CF gives insight into the phase changes occurring during the laser-material interaction, i.e., conversion of material from the nascent solid state to liquid state and then to vapor phase compressing the ambient atmosphere [15,17,25], hence releasing the SF. The SF is observed to get detached from CF at 3.2 μs and 3.6 μs for Al and Ni-Al pellets,

respectively. While for other compacted powders the energy released was observed later than 5 μs . The oscillations of R_{CF} at longer time scales indicate the ablation dynamics of the compacted powders giving an insight into the precise time of energy release. The faster launching of SF into ambient air indicates quicker release of kinetic energy from the Al, Ni-Al compacted nanopowders compared to other powders studied in this work. The R_{CF} is observed to be higher for Al with a maximum radius of 3.1 mm compared to the other materials. Though Ni-Al has higher atomic weight compared to the Al nanopowder presumably leading to a higher ablative pressure [26], Ni-Al has a low ignition temperature compared to Al due to the intermetallic reactions between Al and Ni atoms [2,13]. Moreover, with ns pulses in the visible region, the skin depth of the radiation ensures that Ni coating (~ 15 nm) gets completely ablated shielding the Al particles to the incident laser beam, hence reducing the coupling of laser energy and the resulting ablation rate.

The time dependent evolution of shock front (R_{SW}) allowed us to directly measure the shock velocity (V_{SW}). The pressure behind the SF (P_{SW}) is estimated by using Counter Pressure Corrected Point Strong Explosion Theory (CPC-PSET) taking into account the pressure exerted by the ambient atmosphere on the propagation of shockwave [15–18]. Among the five different compacted pellets, the SW properties are observed to be higher for Aluminum (Al) with the maximum V_{SW} and P_{SW} of 6.2 km/sec and 38 MPa respectively and lower for KBr with the maximum V_{SW} and P_{SW} of 3.7 km/sec and 13 MPa respectively (Figs. 5(a) and 5(b)). Both velocity and pressure behind the SF are observed to decay due to the rapid expansion of the SW with time delay from the laser pulse. At 11.2 μs delay from the laser pulse, SW reaches the acoustic limit (346 m/sec) where the shock pressure reaches to atmospheric pressure (0.1 MPa).

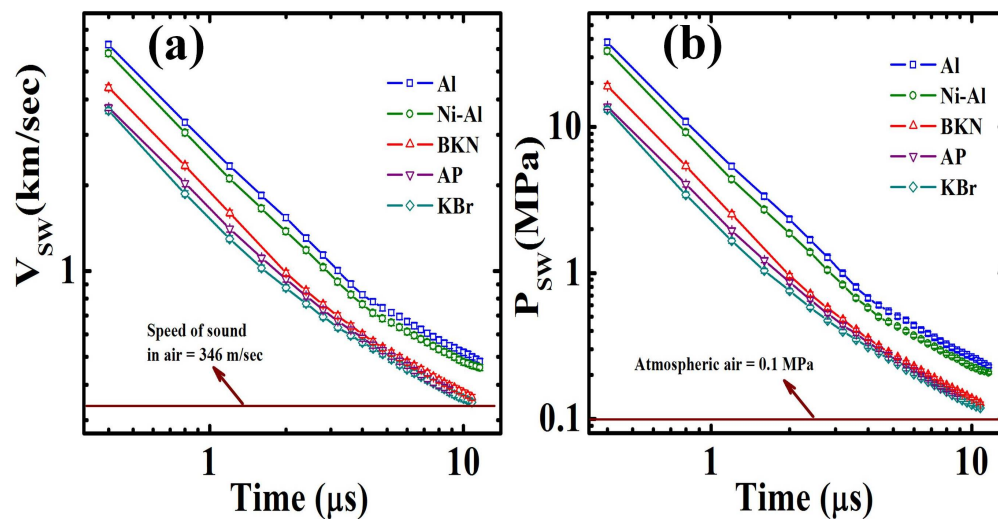


Fig. 5. (a) Velocity (V_{SW}) and (b) Pressure (P_{SW}) behind the shock front (SF) for the compacted materials. Lines are guide to the eye. The horizontal lines in the figures (a) and (b) represent the speed sound and pressure of ambient atmospheric air, respectively.

The specific impulse, I_{SP} taken as V_{SW}/g , where g is the acceleration due to gravity for the compacted powders is in the range of 350 – 650 sec (Table 1). The I_{SP} values of the compacted metal nanopowders are observed to be much higher compared to regular bulk metals [10–13]. This is due to the larger surface area offered by nanopowders that enhance coupling of laser radiation to the material layer leading to increased plasma temperature [27,28] that result in higher ablation and the associated shock emissions.

Table 1. I_{sp} values for different compacted nanopowders at 0.4 μ s delay from the laser pulse

Material	I_{sp} (sec)
Al	634 ± 15
Ni-Al	591 ± 14
BKN	449 ± 11
AP	382 ± 9
KBr	373 ± 9

4. Summary and future scope

Shadowgraphic imaging is used to study the laser ablative shockwave and contact front dynamics from different compacted powders in pellet form such as nano Aluminum (Al), Nickel coated nano Aluminum (Ni-Al), Boron Potassium Nitrate (BKN), Ammonium perchlorate (AP) and potassium Bromide (KBr) targets with ns temporal resolution. Among the five different materials, the SW properties are observed to be higher for nano Al followed by Ni-Al, BKN, AP and KBr. From the time dependent evolution of shock front and the contact front precise time of energy release from the materials and an insight into the dynamics of ejected material launching a shock into the ambient medium is obtained. This allows an option to control the energy release requirements as the shock front can either be accelerated or decelerated by choosing appropriate materials and compositions. The I_{sp} for Al and Ni-Al greater than 500 sec indicate the potential of these compacted metal nanopowders for microthruster applications that lead to environmental friendly applications of energetic materials.

Acknowledgments

The authors thank DRDO, Government of India for Grants-in-Aid Support.